Systems & Control Transactions

Original Research Article
Peer Reviewed Conference Proceeding
ESCAPE 36 - European Symposium on Computer Aided Process Engineering
Sheffield, UK. 21-24 June 2026

PSE PRESS

A Framework for Flexible Start/Stop Operation of Electrified Chemical Processes

Samuel Mercer[a] and Michael Baldea[ab]*

[a] McKetta Department of Chemical Engineering, The University of Texas at Austin, Austin, TX, USA
[b] Oden Institute for Computational Science and Engineering, The University of Texas at Austin, Austin, TX, USA
* Corresponding Author: mbaldea@che.utexas.edu.

ABSTRACT

A flexible start-stop operating policy that involves full shut-down and start-up may be beneficial for electrified plants under certain grid conditions, such as dispatchable demand response. This paper introduces a multi-period Hamilton-Jacobi reachability framework to explore the space of state trajectories for plant shut-down and start-up. Shut-down is defined in terms of operations leading to a stand-by state with no material flows or energy inputs, and variables within safety constraints. Candidate stand-by states are identified by constructing backwards reachability tubes from the desired steady-state operating point. The candidate shut-down/stand-by state is partitioned in fast and slow regions. Admissible control input trajectories are determined for the fast region, from which the minimum time trajectory is selected as optimal for fast start-up. A proof-of-concept simulation using a reaction/separation/recycle plant is presented.

Keywords: Plant Start-up, Process Electrification, Hamilton-Jacobi Reachability, Optimal Control

INTRODUCTION

Electrified processing and, in particular, electrified process heating offer new opportunities for the precise delivery of process energy, enabling faster, smaller, safer, and more efficient processes [1]. Operational flexibility is critically important for electrified processes. With a growing share of electricity generation from renewable sources, characterized by inherent temporal variability, and rapidly increasing demand from large electricity users such as data centers, plants with large electricity loads should have the capability to modulate power consumption in response to grid conditions and (ideally) benefit economically from doing so [1-2]. Modulation typically consists of temporary decreases or increases in production rates when electricity prices are high or low, respectively, as in price-driven demand response; flexible start-stop operation extends this idea, potentially allowing plants to take further advantage of incentive-driven demand side management such as interruptible power [3].

The start-stop operation of a chemical plant is a transient mode of operation that uses start-up and shut-down procedures to temporarily interrupt and (eventually) restart continuous production [3, 4, 5, 6]. Shut-down involves transitioning the plant from the nominal operating state to a passive stand-by state without process (material and energy) flows (and likely without control input). Start-up consists of transitions from the stand-by state back to the nominal state under safety and operability constraints by restarting process flow and control [5, 6]. For continuous processes, such events are typically rare and restricted to maintenance or emergency situations. The loss of production over the start-stop period, high energy requirements to restart process units (e.g., staged units such as distillation columns) and long start-up durations are costly. Nevertheless, fast start-stop operations (where the cycle occurs over a time interval that is relevant to daily fluctuations in electricity prices) could have substantial benefits [1, 2].

Motivated by the above, the contribution of this work is to develop an analysis framework for start-stop operations based on Hamilton-Jacobi reachability. We are specifically interested in describing the "stopped/stand-by" state that meets the above conditions and results in the fastest startup and restoration of the nominal operating state. A case study on the start-up of a simple reactor/separation/recycle process illustrates

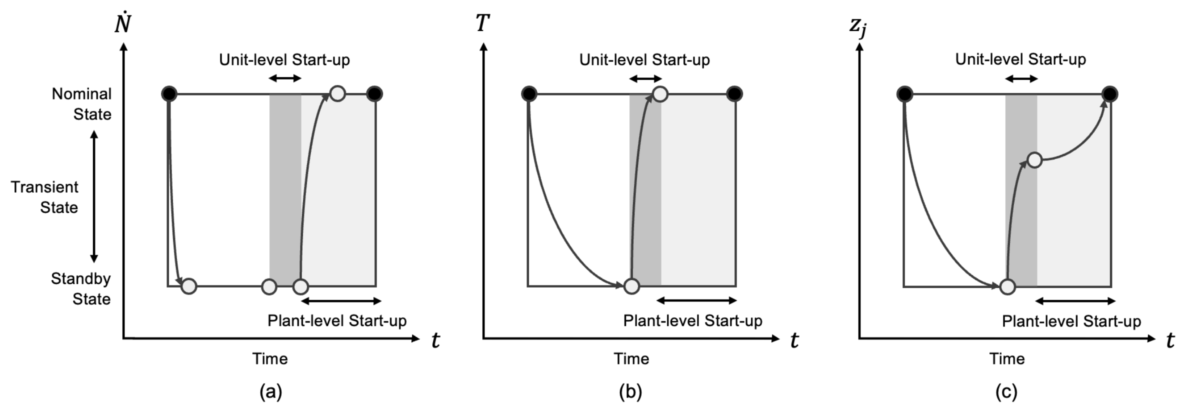

Figure 1. Schematic of the state trajectories for the (a) flow rate, (b) temperature, (c) composition for component *j* over a full shut-down and start-up cycle. The white region signifies the shut-down and stand-by period, the dark gray region the feed ramp-up start-up period, and the light gray region the composition control start-up period. The temperature is restored to its nominal operating state quickly followed by the flow rate, while the composition is the slowest.

the framework.

PLANT START-STOP OPERATIONS

Plant *start-stop* operations define a full shut-down to start-up cycle where the plant temporarily stops material and energy flow. To guide the discussion, the state trajectories of the flow, temperature, and composition variables are shown in Figure 1 for the full cycle. We define the following cycle periods:

Shut-down: starting from nominal steady-state operating conditions, the plant stops production by closing feed and product streams. The closed plant gradually shuts interconnections between individual units (or subsystems).

Stand-by: individual units operate as autonomous closed systems without control action. The state derivatives are near zero and the holdup is at a near constant value. Control inputs are disabled and units are not interconnected. Material holdup is redistributed due to pressure and/or temperature gradients, resulting in changes in internal flow traffic such as draining in staged systems, pressure losses, or backmixing due to condensation. Energy is lost in the form of passive cooling from heat dissipation. The longer the standby period, the farther each sub-system drifts from the nominal steady-state operating point.

Unit-level Start-up: each unit starts up individually, similar to a batch operation, as their control inputs are reactivated. Their state progresses towards an intermediary (local) operating point that precedes plant-wide interconnection. This period ends when the slowest unit reaches its local operating point.

Plant-level Start-up: interconnections are re-established between local sub-systems to form the global system. Feed and product streams are re-introduced as well as feedback interconnections, such as recycle loops. The plant returns to the nominal steady-state driven by the manipulated variables, as dictated by a control system and/or operator inputs. The full shut-down-startup cycle is complete once the system returns to its nominal steady-state. It is assumed that the steps taken in the start-up and shut-down procedures are known (i.e., we are not attempting to devise new procedures).

CONCEPT: REACHABILITY FRAMEWORK

Efficient and timely start-stop operations depend on finding a (set of) plant state(s) that meet the description of the stand-by state, and for which feasible trajectories exist to and from the nominal operating state.

Hamilton-Jacobi (HJ) reachability analysis [8, 9, 10] is a powerful global method to explore all possible paths between two operating points, that satisfy system constraints. It comprises of formulating a forward or backward problem that derives feasible state trajectories over a finite time horizon, subject to an admissible control input trajectory. The forward problem maps all reachable final states from an initial state. The backward problem starts from the target set and maps the set of all initial states that reach the target, which is termed as the attraction basin. For start-stop operations, we formulate the backward reachability problem as the target operating state (i.e., the nominal state), which is known *a priori*.

On a related note, HJ backward reachability is closely related to minimum-time optimal control. There may exist an initial state and some admissible control

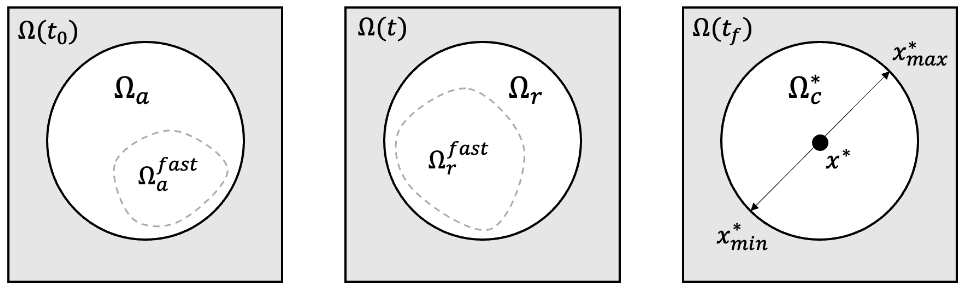

(a) (b) (c)

Figure 2. Plant abstract operating space Ω cross-sections for (a) the attraction basin Ω_a with fast region Ω_a^{fast} at initial time t_0, (b) the reachable set Ω_r with fast region Ω_r^{fast} at some intermediate time t , and (c) the capture basin Ω_c^* at terminal time t_f containing the target set x^*.

trajectory that reaches the target set the fastest. For plant-wide start-up, we aim to identify this path.

MATHEMATICAL FORMULATION

Plant Network Dynamics

Consider a plant with $i = 1, \dots, N_{units}$ process units, where each unit has state variables $x \in \mathbb{R}^m$ in the vector $\mathbf{x}$ and control inputs $u \in \mathbb{R}^p$ in the vector $\mathbf{u}$ given by:

$$\dot{\mathbf{x}}(t) = f(\mathbf{x}, \mathbf{u}, t) \quad (1)$$

over the finite time horizon $t: [t_0, t_f]$, where t_0 and t_f represent the initial and final times, respectively. x and u have operability constraints $x_{min} \le x \le x_{max}$ and $u_{min} \le u(t) \le u_{max}$, which are valid for all time [11, 12]. The maximum allowable time horizon τ satisfies $\tau \ge t_f - t_0$. The state trajectory ϕ is defined as:

$$x(t) = \phi(t, t_0, x_0; u(t)) \quad (2)$$

while u has an admissible control trajectory ϕ^{u}:

$$u(t) = \phi^u(t, t_0, u_0; x(t)) \quad (3)$$

The plant network is a collection of process units with a set of state variables $\Omega = [\mathbf{x}_1, \mathbf{x}_2, \dots, \mathbf{x}_{N_{units}}]^T \in \mathbb{R}^{N_{units} \times m}$ and set of control inputs $\Omega^{\mathrm{u}} = [\mathbf{u}_1, \mathbf{u}_2, \dots, \mathbf{u}_{N_{units}}]^T \in \mathbb{R}^{N_{units} \times p}$:

$$\dot{\Omega}(t) = (I \otimes A + \gamma(t) \otimes \zeta(t))\Omega(t) + (I \otimes B)\Omega^{\mathrm{u}}(t) \quad (4)$$

where $A \in \mathbb{R}^{m \times m}$ is a state matrix, $\gamma(t) \in \mathbb{R}^{N_{units} \times N_{units}}$ is a graph Laplacian matrix defining the connectivity of the network topology, $\zeta(t) \in \mathbb{R}^{m \times m}$ is a coupling matrix between the state variables of connected process units, B is a control input matrix, and I is the identity matrix, all of appropriate dimensions.

Equivalently, the plant state trajectory $\Phi \in \mathbb{R}^{N_{units} \times m}$ is defined as:

$$\Omega(t) = \Phi(t, t_0, \Omega(t_0); \Omega^{\mathrm{u}}) \quad (5)$$

where $\Omega(t_0)$ is the set of initial states for all state variables. Ω^{u} has an admissible plant control trajectory Φ^{u}:

$$\Omega^u(t) = \Phi^u(t, t_0, \Omega^u(t_0); \Omega(t)) \quad (6)$$

Backward Reachability

Ω^* is a target steady-state operating region that consists of a subset of target state variables x^* subject to production and quality constraints $x^*_{min} \le x^* \le x^*_{max} \in \mathbb{R}^m$ (Figure 2c). The capture basin Ω_c^* is the region of state space enclosing x^* such that $x^* \in \Omega_c^*$. It is implied that Ω_c^* is a terminal condition that is reached at $t = t_f$ such that $\Omega_c^* \subset \Omega(t_f)$. It is also assumed that x^* exists on a stable equilibrium manifold.

A state $\Omega(t_0)$ is backward reachable from Ω_c^* if there exists an admissible control trajectory Φ^{u} such that the state trajectory Φ reaches Ω_c^* within the finite time horizon satisfying $\tau \ge t_f - t_0$. The attraction basin $\Omega_a(t_0, \Omega(t_0))$ (Figure 2a) consists of the set of initial states that are backward reachable.

Ω_a can be extended to become a backward reachability tube $\mathcal{B}$ (Figure 3), which is defined as the collection of Ω_a for some intermediate time on the interval $[t_0, t_f]$ that reaches x^*:

$$\mathcal{B} = \bigcup\nolimits_{t \in [t_0, t_f]} \Omega_{\mathrm{a}}(t, \Omega^*) \times \{t\} \quad (7)$$

For each $\Omega_a \in \mathcal{B}$, the mapping from Ω_a to Ω_c^* contains a set of admissible state and control trajectories that span a range of reachable states $\Omega_r(t, t_0, \mathcal{B})$ (Figure 2b) within the operable state space. The reachable space Ω_r over τ is therefore:

$$\Omega_r(\Omega(t_0)) = \bigcup\nolimits_{t \in [t_0, t_f]} \mathcal{B}(t, t_0) \quad (8)$$

which implies $\Omega_r \subseteq \Omega$.

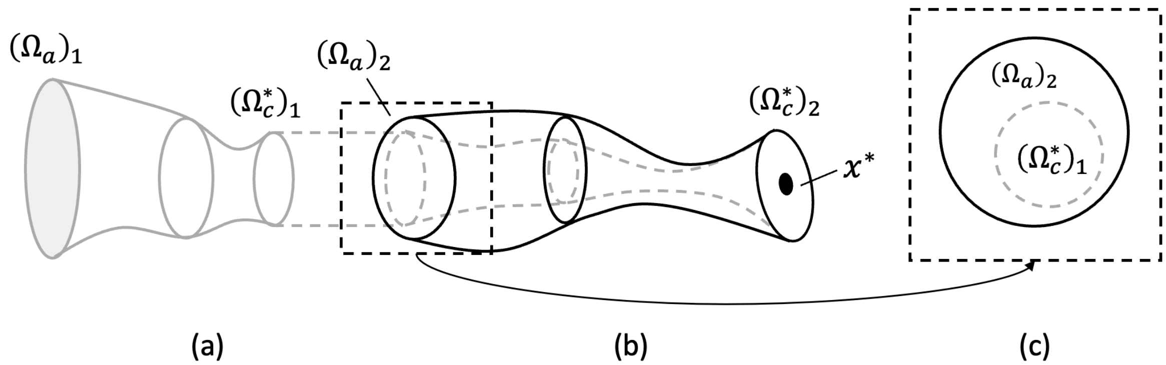

Figure 3. The backward reachability tube $\mathcal{B}$ for (a) $\mathcal{B}_1$ feed ramp-up start-up period (indexed by 1 and colored in gray solid lines) and (b) $\mathcal{B}_2$ composition control start-up period (indexed by 2 and black solid lines). The attraction and capture basins for each period are visible at an intermediary operating point, where the intersection between $(\Omega_a)_2$ and $(\Omega_c^*)_1$ (Equation 12), as shown in (c), forms a reachable multi-period tube (traced by the gray tube in solid lines for $\mathcal{B}_1$ and dashed lines for $\mathcal{B}_2$).

Minimum Time Optimal Control

The backward reachability tube (BRT) is computed using Hamilton-Jacobi reachability theory. The first step is to define an implicit level set function Ψ to define the proximity of the current state $x(t)$ from x^* for all $x^* \in \Omega^*$:

$$\Psi = \left|x - \frac{x^*_{min}+x^*_{max}}{2}\right| - \frac{x^*_{min}-x^*_{max}}{2} \quad (9)$$

Equation 9 suggests that if $\Psi \leq 0$, then x is within Ω_c^*. This implies that Ψ encodes $\mathcal{B}$; it is also equivalent to the value function V in the constrained Hamilton-Jacobi-Bellman partial differential equation (HJB-PDE, Equation 10a) with terminal condition (Equation 10b), which computes the manipulated input trajectory that reaches the target set the fastest:

$$\frac{\partial V}{\partial t}(t,x) + \min_u \left(\nabla V(x(t),t) \cdot f(x,u,t)\right) = -1 \quad (10a)$$

$$V(x(t_f),t_f) = \Psi(t_f) \quad (10b)$$

The optimal admissible control trajectory for each possible initial state $x(t_0)$ can be derived from Equation 10 for minimum time:

$$u^*(t,x) = \underset{u}{\operatorname{argmin}}\left(\nabla V(x(t),t) \cdot f(x,u,t)\right) \quad (11)$$

which is measured by the reachability time τ^* for each initial state given u^*, where $\tau^* \leq \tau$ and is defined as the time interval for a trajectory to reach Ω_c^* from some initial state. The u^* for each process unit constitutes the set Ω^u.

After V is computed, the BRT may be partitioned between fast and slow regions based on the reachability time τ^*. The smallest τ^* corresponds to the fastest start-up time. As such, the initial state $\Omega(t_0)$ lying within the fast region of Ω_a, denoted by Ω_a^{fast}, and its corresponding minimum-time control trajectory Ω^u with the fastest state trajectory Ω is equivalent to the minimum-time optimal control solution.

Multi-Period Reachability

The above approach for one time period can be extended to multiple time periods. Discrete behavior for start-stop operations, such as alterations to the process topology (e.g. turning on specific units or enabling/disabling streams), can be split into $k = 1, \ldots, N_{period}$ periods. The connection between periods are intermediary operating points that intersect the attraction basin of the k^{th} period $(\Omega_a^*)_k$ and capture basin of the k-1 period $(\Omega_c^*)_{k-1}$, as visualized in Figure 3c.

Remark: the operating spaces in Figure 2 show one step in the backward reachability for each time period τ_k, as reflected in Figure 3.

$$(\Omega_c^*)_{k-1} \cap (\Omega_a^*)_k \quad (12)$$

Thus, a reachable multi-period tube assumes that the intersection in Equation 12 is non-empty, otherwise the multi-period tube does not exist.

Start-up Reachability

Plant start-up reachability is represented by the possible backward paths from the nominal state to the stand-by state. The following framework is proposed to map reachable and optimal trajectories:

(1) Identify the region of possible stand-by states.

(2) From the nominal steady state, identify each step in the operating sequence and their intermediary operating points based on where discrete behavior arises (Figure 3b). Examples are feed ramp-up or turning on control valves.

(3) Validate the connectivity between time periods based on Equation 12 (Figure 3c) to fully trace the $\mathcal{B}$ from the desired/target state. Work backwards until reaching the initial start-up state, which corresponds to the final stand-by state. The state derivatives are near zero and the holdup is at a constant value. Control inputs are disabled and units are not interconnected.

(4) Determine where the region of possible stand-by states in Step (1) intersect with $(\Omega_a)_1$, as depicted in in Figure 3a. This is the region in the state space that is the most favorable stand-by region for fast start/stop operation where there exists fast and slow regions.

(5) Identify the fast and slow regions based on the total time to reach steady-state from the grid of all feasible initial conditions (Figure 2a) for each time period. The full start-up time is given by the sum of τ_k for each period.

CASE STUDY

Consider a prototype reactor-recycle-separation system with purge (shown in Figure 4), similar to systems found in [13, 14]. Assume the following: the holdup is constant for all units (and, therefore, the collective plant holdup), the temperature is constant, and the energy balance is neglected. The authors recognize that this may not be fully representative of electrified processes, where it is likely that the largest use of electricity will be in the form of process heat. Nevertheless, the features highlighted here are broadly applicable.

The process has two components: A and B, where B is the desired product. The composition variables are subject to constitutive relations:

$$1 = x_{A1} + x_{B1} \tag{13}$$

$$1 = x_{A2} + x_{B2} \tag{14}$$

x_{A1} and x_{A2} are differential variables of component balances:

$$\frac{d}{dt}\begin{bmatrix} x_{A1} \\ x_{A2} \end{bmatrix} = \begin{bmatrix} -\frac{F_1}{N_1} - k_1 & \frac{\alpha_A R}{\beta N_1} \\ \frac{F_1}{N_2} & -\frac{F_2}{N_2} - \frac{\alpha_A F_3}{\beta N_2} \end{bmatrix} \begin{bmatrix} x_{A1} \\ x_{A2} \end{bmatrix} + \begin{bmatrix} \frac{F_0 x_{A0}}{N_1} \\ 0 \end{bmatrix} \tag{15}$$

The overall plant material balance is between the feed F_0, product F_2, and purge P streams

$$F_0 = F_2 + P \tag{16}$$

$$P = \lambda F_3 \tag{17}$$

where P is determined by the split ratio λ between the vapor stream F_3 and the recycle stream R

$$R = (1 - \lambda) F_3 \tag{18}$$

F_0 is pure A ($x_{A0} = 1$) and mixes with R (whose composition is x_{A3} and x_{B3}). The combined stream $F_0 + R$ enters a liquid phase reactor (indexed as Unit 1) where A converts to B in an irreversible forward reaction $A \rightarrow B$.

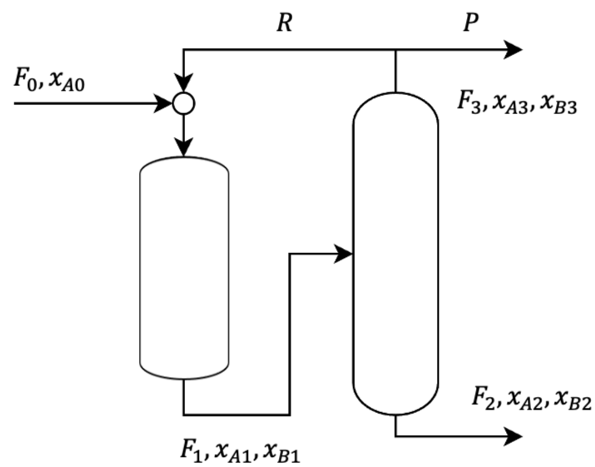

Figure 4. Chemical plant with a reactor, a flash drum, a recycle stream, and a purge stream.

$$\frac{d}{dt}(N_1) = 0 = F_0 + R - F_1 \tag{19}$$

The reactor outlet stream F_1 has composition x_{A1} and x_{B1}, and feeds into a single stage separator (indexed as Unit 2) that splits F_1 into a liquid product stream F_2, which concentrates the desired product B, and a vapor stream F_3 that concentrates the unreacted A.

$$\frac{d}{dt}(N_2) = 0 = F_1 - F_2 - F_3 \tag{20}$$

The flash calculation in the separator is computed using a linearized Rachford-Rice equation, where α_A and α_B represent the relative volatility of components A and B while β represents a phase transfer coefficient.

$$0 = \frac{x_{A2}}{(1-\alpha_A\beta^{-1})^{-1} - F_3 F_1^{-1}} + \frac{x_{B2}}{(1-\alpha_B\beta^{-1})^{-1} - F_3 F_1^{-1}} \tag{21}$$

$$\beta = \alpha_A x_{A2} + \alpha_B x_{B2} \tag{22a}$$

$$x_{A3} = \frac{\alpha_A}{\beta} \tag{22b}$$

$$x_{B3} = \frac{\alpha_B}{\beta} \tag{22c}$$

The plant start-up comprises of manipulating the split ratio λ to control the purity of the separator product stream during the feed ramp-up and composition control periods. The goal is to identify the stand-by region that allows startup, as well as the subregion for the fastest startup. The model parameters are available in Table 1.

Table 1: Model parameters.

Symbol	Parameter	Value
α_A	Relative volatility of A	10.5
α_B	Relative volatility of B	3
F_0^{nom}	Nominal feed flow rate	25 kmol/hr
N_1	Reactor holdup	50 kmol
N_2	Drum holdup	45 kmol
k_1	First-order rate constant	10 s^{-1}
x_{A1}	A mole fraction (reactor)	0.5
x_{A2}	B mole fraction (drum)	0.8
t_f	Time horizon	6 hr

Numerical Implementation

A dynamic programming approach is adopted to efficiently solve the finite horizon HJB equation. The state and time variables of Equation 10 are discretized where x_{A1} in $m = 0, \dots, N_{x_{A1}}$ grid points and x_{A2} in $n = 0, \dots, N_{x_{A2}}$ grid points. The new discrete variables are x_{A1}^m and x_{A2}^n. The control variable λ is discretized in $l = 0, \dots, N_\lambda$ grid points, to form the discrete control set λ^l. Piecewise-constant controls are used, updated on an interval of Δt_c.

The value function is defined as follows:

$$V_{nm}(t_f) = \begin{cases} 0, x \in \Omega_c^* \\ \infty, x \notin \Omega_c^* \end{cases} \tag{23}$$

There are two distinct time discretization schemes. An explicit backward Euler integration scheme for Δt steps is applied to discretize the process dynamics:

$$\frac{dx_{A1}}{dt} = \frac{x_{A1}^{t+1} - x_{A1}^t}{\Delta t} \tag{24}$$

$$\frac{dx_{A2}}{dt} = \frac{x_{A2}^{t+1} - x_{A2}^t}{\Delta t} \tag{25}$$

and a semi-Lagrangian backward propagation scheme of the HJB equation for Δt_c steps over the control trajectory [15].

$$V_{nm}^{t_c+1} = \min_{\lambda^l}\left[\Delta t_c + V_{nm}^{t_c}\right] \tag{26}$$

The full λ^l space is recursively searched for a time-optimal control λ_{nm}^{l*}:

$$\lambda_{nm}^{l*} = \operatorname*{argmin}_{\lambda^l}\left[\Delta t_c + V_{nm}^{t_c}\right] \tag{27}$$

The numerical settings are specified in Table 2. All computations were performed using Python 3.13.5 and NumPy 2.1.3. The runtime was 6 minutes.

Table 2: Numerical settings.

Symbol	Parameter	Value
$N_{x_{A1}}$	x_{A1} grid resolution	120
$N_{x_{A2}}$	x_{A2} grid resolution	120
Δt	Euler time step size	0.05
Δt_c	Control time step size	0.2

Results

The purity set-point is 0.95 mol% for x_{B2}. Figure 5 shows the shape of the BRT (as anticipated in Figure 3a and 3b) and the intersection of the tubes for each period, tracing a full feasible BRT for start-up. Figure 6 compresses the BRT onto a 2D grid for each period.

In Figures 6a-i and 6a-ii, the attraction basin expands as the time horizon increases, implying that more initial states are reachable for longer times. Considering that the holdup is constant, the feedback from the recycle stream shows how the initial holdup composition in the reactor and separator affects the start-up length. The boundary of the attraction basin expands to more initial x_{A2} states at higher initial x_{A1} for a given time. While this is intuitive, we find the converse perspective more useful: the state space region that allows for fast start-up becomes narrower as the desired start-up time gets shorter.

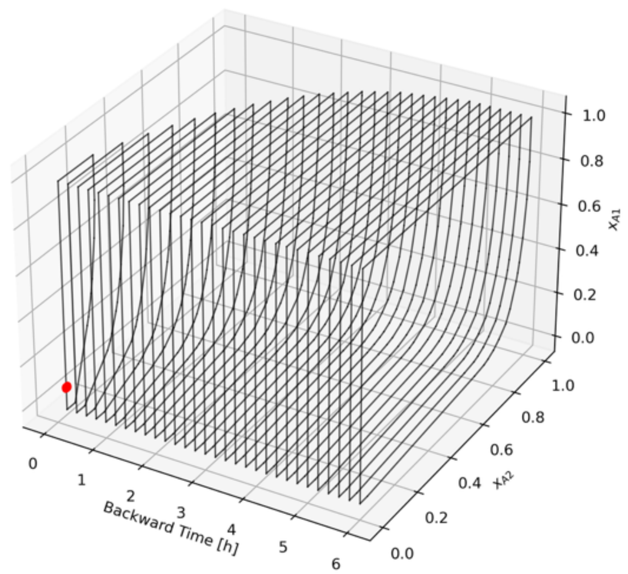

Figure 5. Backwards reachability tube for the start-up of the reactor-recycle-separation system. The red dot denotes the target set x^*.

Figures 6b-i and 6b-ii illustrate the optimal time-averaged split ratio for each initial state. Higher x_A initial reactor concentrations, which are far from the nominal state, taper towards $\lambda = 0$ and favor recycle-only operation. Purge-only operation $\lambda = 1$ is favored when x_{A1} is near the target operating state. Alternative split ratios are favored over the interval $x_{A1} = [0.2, 0.5]$.

Remark: In Figures 5 and 6, the discretization scheme is a coarse-grained approximation of the attraction basin and set of recycle ratios, which is why the profiles have streaks along the basin boundary. A finer approximation with more grid points would generate a smoother profile but would require longer computational time.

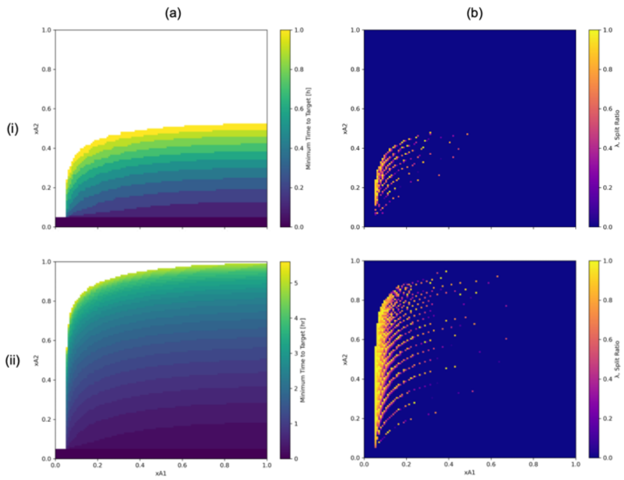

Figure 6. Set of (a) attraction basins and (b) optimal split ratios for (i) feed ramp-up period and (ii) composition control period.

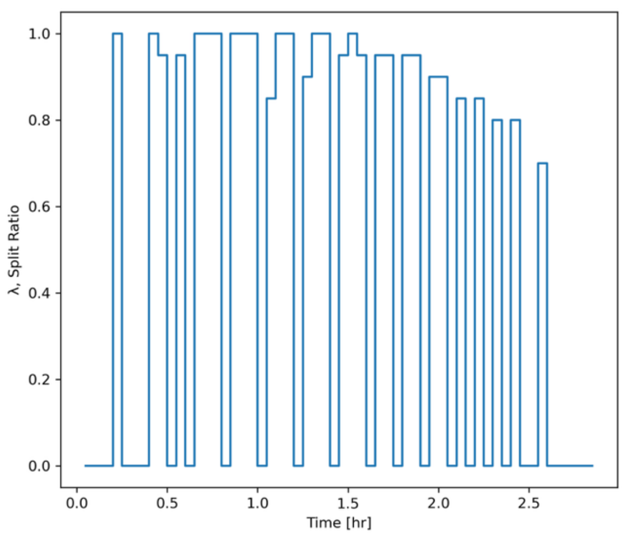

Figure 7. Optimal control trajectory of the split ratio during the composition control period.

From the results in Figures 5 and 6, let us consider an initial state of $[x_{A1,0} = 0.9, x_{A2,0} = 0.9]$ whose total start-up time is 2.6 hr. An optimal control trajectory for the split ratio is presented in Figure 7, where there is initially large variation until the system reaches the nominal steady state. The optimal trajectory is reflected in the black-colored trajectory on the phase portrait shown in Figure 8. Notably, state trajectories from all initial conditions converge to the same path to the capture basin. The proposed framework provides a full view of the feasible operating space under operability and finite time constraints. It is shown how the feasible state and control trajectories are systematically determined by a global exploration of the control space. Provided the shape of the BRT and its associated attraction basins, the initial state (which is, in fact, the stand-by state of the plant) has a substantial impact on the start-up speed. The ability to confine the process unit state to the fast region of an attraction basin during shut-down and stand-by has a great effect on start-up, suggesting that an interruptible operation is governed as much by its available control inputs as the ability to maintain the system state near the target conditions.

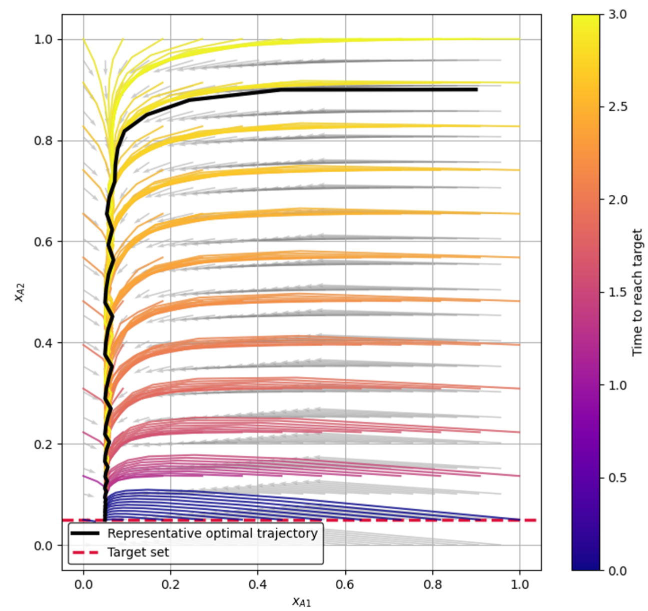

Figure 8. Phase portrait of control trajectories during composition control period. The black trajectory is an optimal path given the initial state (x_{A1} = 0.9, x_{A2} = 0.9) from stand-by.

CONCLUSIONS AND FUTURE WORK

In this paper, a conceptual framework for analyzing start-stop operations was developed based on Hamilton-Jacobi reachability. Attraction basins were found by deriving backward reachability tubes from a target set, from which the fast region of the attraction basin was identified. Within this region, the optimal admissible control trajectory corresponding to the fastest state evolution is found. A plant start-up case study for reactor/separation/recycle focusing solely on composition dynamics was demonstrated as a proof-of-concept. The next step is to validate the proposed framework on an industrial system with higher dimensionality.

ACKNOWLEDGEMENTS

This work was supported by the National Science Foundation Graduate Research Fellowship Program

(GRFP) and the Provost's Graduate Excellence Fellowship at the University of Texas at Austin. This material is based upon work supported by the U.S. Department of Energy's Office of Energy Efficiency and Renewable Energy (EERE) under the Industrial Technologies Office (ITO), Award Number DE-EE0010725. The views expressed herein do not necessarily represent the views of the U.S. Department of Energy or the United States Government.

AUTHOR IDENTIFIERS

Author ORCIDs:
Mercer SP: 0000-0003-3224-5670
Baldea M: 0000-0001-2345-6789

REFERENCES

1. Baldea M, Endler EE, Hale E, Maravelias CT, Barolo M, Harjunkoski I, Mercangoz M, Shah SL, Soroush M, Young BR, Zhang Q. Transforming the process industries through electrification: challenges and opportunities. Ind. Eng. Chem. Res. 64:16466-16478 (2025). https://doi.org/10.1021/acs.iecr.5c01256
2. Harjunkoski I, Vaara S. Demand-side opportunities for process industry participation in electricity markets. Ind. Eng. Chem. Res. 64:24675-24688 (2025). https://doi.org/10.1021/acs.iecr.5c03604
3. Zhang Q, Morari MF, Grossmann IE, Sundaramoorthy A, Pinto JM. An adjustable robust optimization approach to scheduling of continuous industrial processes providing interruptible load. Computers & Chemical Engineering 86:106-119 (2016). https://doi.org/10.1016/j.compchemeng.2015.12.018
4. Chong, Z. Dynamic optimization formulations for plant operation under partial shutdown conditions. McMaster University PhD Dissertation (2012).
5. Durkin, A, Stolte, J, Mercangöz, M. Hoflon: hybrid offline learning and online optimization for process start-up and grade-transition control. *arXiv preprint* (2025).
6. Srinivasan R, Viswanathan P, Vedam H, Nochur A. A framework for managing transitions in chemical plants. Computers & Chemical Engineering 29:305-322 (2005). https://doi.org/10.1016/j.compchemeng.2004.09.024
7. Verwijs JW, van den Berg H, Westerterp KR. Startup strategy design and safeguarding of industrial adiabatic tubular reactor systems. AIChE Journal 42:503-515 (2004). https://doi.org/10.1002/aic.690420219
8. Kanavalau A, Lall S. Thermal runaway avoidance using hamilton–jacobi reachability and model predictive control. Computers & Chemical Engineering 157:107605 (2022). https://doi.org/10.1016/j.compchemeng.2021.107605
9. Kurzhanski AB, Varaiya P. Trajectory tubes state-constrained feedback control. Systems & Control: Foundations & Applications :311-339 (2014). https://doi.org/10.1007/978-3-319-10277-1_8
10. Yin H, Arcak M, Packard A, Seiler P. Backward reachability for polynomial systems on a finite horizon. IEEE Trans. Automat. Contr. 66:6025-6032 (2021). https://doi.org/10.1109/tac.2021.3056611
11. Dinh S, Lima FV. Dynamic operability analysis for process design and control of modular natural gas utilization systems. Ind. Eng. Chem. Res. 62:2052-2066 (2023). https://doi.org/10.1021/acs.iecr.2c03543
12. Dinh S, Lima FV. Linear dynamic operability analysis with state-space projection for the online construction of achievable output funnels. Computers & Chemical Engineering 205:109428 (2026). https://doi.org/10.1016/j.compchemeng.2025.109428
13. Falcone M, Ferretti R. Semi-lagrangian approximation schemes for linear and hamilton—jacobi equations. Society for Industrial and Applied Mathematics (2013). https://doi.org/10.1137/1.9781611973051
14. Baldea M, Daoutidis P. Dynamics and nonlinear control of integrated process systems. Cambridge University Press (2012). https://doi.org/10.1017/cbo9780511978760
15. Zhang J, Liu J. Distributed moving horizon state estimation for nonlinear systems with bounded uncertainties. Journal of Process Control 23:1281-1295 (2013). https://doi.org/10.1016/j.jprocont.2013.08.005